Laser printing of silicon-containing multilayer anodes with optimized electrode inks

U. Rist*, W. Pfleging
Karlsruhe Institute of Technology, IAM-AWP, P.O. Box 3640, 76021 Karlsruhe, Germany

ABSTRACT

The demand for improved and affordable batteries is increasing with the further decarbonization of mobility and other parts of the industry. To further improve lithium-ion technology, high-capacity materials such as silicon must be introduced to increase the energy density of the batteries. Furthermore, customized electrode architectures can help to improve the cycle stability and thus increase the acceptance for batterie powered mobility and mobile devices. For this purpose, multilayer electrodes were printed with the laser-induced forward transfer process, using inks with different active materials for the different layers. As active materials the high-capacity material silicon and the state-of-the-art material graphite were used. The electrodes were assembled in coin cells against lithium and were electrochemically analyzed. The prepared cells have twice the specific capacity compared to pure graphite electrodes due to the addition of silicon. After cycling, the cells were disassembled. Here, no lithium plating or deformation of the current collector was detected.

Keywords: Laser-induced forward transfer, anode printing, lithium-ion battery, 3D battery, multilayer, silicon, graphite, additive manufacturing

1. INTRODUCTION

The demand for improved and affordable batteries is increasing by the growing number of battery powered devices. So far, the lithium-ion battery is one of the promising electrical-storage technology, but further improvements must be made regarding the volumetric and gravimetric capacity of the cells. Therefore, silicon can be introduced on the anode side as high capacity material with a theoretical capacity of 3579 $mAh \cdot g^{-1}$ [1], which is one order of magnitude higher than the commonly used graphite (372 $mAh \cdot g^{-1}$) [2]. However, silicon undergoes a volume expansion of up to 300 % during lithiation which leads to tremendous mechanical load and thus to a significant reduction in battery lifetime [3]. Here, 3D electrode architectures, like line patterns, can reduce the compression load by offering space for the volume expansion and so increase the battery lifetime [4, 5]. Also, multilayer electrodes are in the focus of research to combine different properties of materials in electrodes [6-8]. Printing technologies can further improve the development of electrode architectures by rapid prototyping [9, 10]. Since laser-induced forward transfer (LIFT) is a nozzle-free technique [11] and a wide range of viscosities [12] and particle sizes can be used. Due to the wide range of possibilities, it offers a flexible tool for electrode printing. Lithium-cobalt oxide (LCO) and graphite micro batteries [13], lithium nickel manganese cobalt oxides (NMC111) cathodes [14], graphite electrodes [6, 9, 15], multilayer electrodes [6, 15], and more complex electrode architectures [16] were already prepared using the LIFT-process. In a previous work [15], polyvinylidene difluoride (PVDF) was used as binder for printing a multilayer silicon-containing anodes. Due to the fact that PVDF binds the particles just by van der Waals forces the binding strength is too weak for withstanding the volume expansion of silicon. Polyacrylic acid (PAA) was used as binder for the electrodes in this work, which is due to stronger binding forces, like hydrogen bonds and covalent interactions, an often-used binder for silicon-containing electrodes [17-21]. In order to investigate the impact of the localization of the different layers, electrodes with two layers were printed. One layer consisted exclusively of graphite as active material and the other layer contains silicon. The printed electrodes were assembled in coin cells and cycled at a C-rate of C/10. After reaching end-of-life the cells were disassembled and analyzed.

*ulrich.rist@kit.edu; phone: +49 721 608 28161

2. EXPERIMENTAL SET-UP

A representative schematic view of the used setup for the LIFT-process is displayed in Figure 1. As laser source a tripled-frequency Nd:YAG laser (Lumentum, San Jose, CA, model: Q301-HD-1000R) with an operating wavelength of 355 nm was used. The laser has a maximum power of 10 W, a maximum repetition rate of 30 kHz and a pulse length of 78 ns. A diffractive optical element (DOE) shapes the Gaussian laser beam profile to a top-hat one. Following the DOE, the laser beam geometry can be shaped into different sizes of rectangles or circles using a mask selector. However, for this work the raw beam, a rectangle with a side length of 175 µm, was used. The beam is illuminated by an objective onto the interface between the quartz glass wafer (DSP-200×0675-SGQ-00, Wafer Universe, Elsoff, Germany) and the electrode ink with a demagnification factor of 3.5. The graphite paste was coated with a doctor blade gap of 40 µm onto the quartz glass wafer. For the silicon containing slurry a gap of 20 µm was applied. As substrate a 9 µm thick copper foil was used.

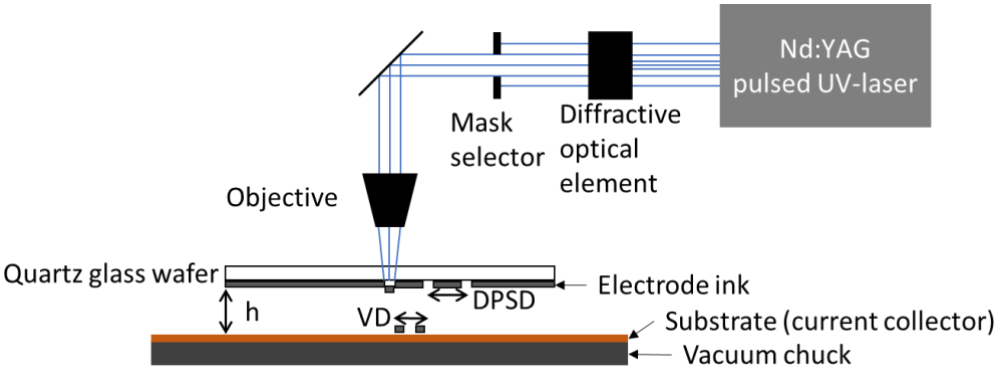

Figure 1: Schematic representation of the used setup for the LIFT-process, based on [6].

The LIFT-process is performed according to the principle of fluid printing described by Fernández-Pradas [22]. The illumination of the laser sublimates parts of the printing ink at the interface between the quartz glass wafer and the printing ink. The resulting gas bubble expands and induces a material (voxel) transfer towards the substrate.

The graphite-containing ink consists of 93 % flake-like graphite (T808, Targray, Kirkland, QC, Canada) as active material, 1.4 % conductive carbon (Super C65, MTI, Richmond, CA, USA) to increase the conductivity of the layer, and 5.6 % PAA (181285, Merck KGaA, Darmstadt, Germany) as binder. The silicon-containing slurry has 40 % silicon (SI-15008, Targray, Kirkland, QC, Canada, d_{50} = 72 nm) as active material, 40 % conductive graphite (KS6L, Imerys, Paris, France) to increase the conductivity but it also takes part at the electrochemical process, and 20 % PAA as binder, which is more suitable for silicon-containing electrodes compared to PVDF.

After cutting the electrodes with an ultrashort pulsed laser (Tangerine, Amplitude Systèmes, Pessac, France, λ = 515 nm) the electrodes were assembled in coin cells (CR2032) with a Celgard 2500 (Celgard LLC, Charlotte, NC, USA) separator and an electrolyte consists of a mixture of ethylene carbonate and ethyl methyl carbonate in a mass ratio of 3:7 with 1.3M $LiPF_6$ with 5 wt.% fluoroethylene carbonate (FEC) as additive (Solvionic, Toulouse, France). Subsequently, they were electrochemically characterized using an Arbin system (BT2000, Arbin Instruments, College Station, TX, USA) according to the electrochemical priming and the long-term test at a C-rate of C/10 as described in [23]. Followed by a short C-rate analysis varying the applied C-rates from C/5 up to 1C. The C-rate is defined by the reciprocal time needed for charging or discharging the cell, means with the C-rate of C/5 it takes 5 hours for charging or discharging.

3. RESULTS AND DISCUSSION

For the analysis of the dependency of the silicon-layer location in multilayer electrodes, one layer graphite ink and one layer silicon-containing ink were printed. There are two different arrangement possibilities for the location of the silicon-containing layer, in direct contact with the current collector (ML1) and on the top of the electrode (ML2). Cross-sectional views of the electrodes are displayed in Figure 2.

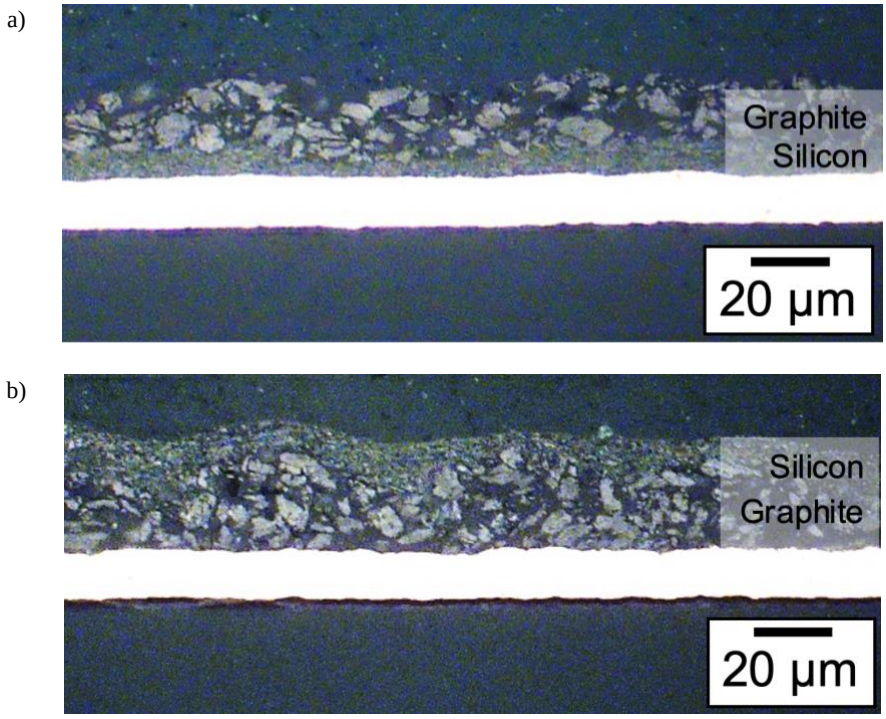

Figure 2: Cross-sectional view of the manufactured electrodes, a) ML1 with silicon-containing layer in direct contact with the current collector, b) ML2 with silicon as the top layer.

In Figure 2a, the cross-section of ML1 is displayed. Here it can be seen, that the bottom layer consist of particles with a much lower particle size than the top layer, which in the latter case is silicon and the top layer is graphite. With ML1, the idea was that the lithium-ions can pass through the graphite layer well, but the silicon could lose adhesion to the current collector due to its volume change during cycling. In ML2 the bottom layer was printed with the graphite ink and on top the LIFT process was performed with the silicon-containing ink. With ML2, the idea was that the adhesion to the current collector is good due to the graphite as the bottom layer, but the silicon could close the pores on the surface. To calculate the material composition of the printed multilayer electrodes in one printing step also areas with only the bottom layer were printed. The mass of the one-layer electrode (bottom layer) and the total mass of the multilayer electrode were used to determine how much mass originated from each layer. The calculated results are displayed in Table 1.

Table 1: Calculated material composition of the multilayer electrodes

Material	**ML1** **\wt.%**	**ML2** **\wt.%**
T808	64.3	64.2
Silicon	12.3	12.4
Conductive additive	13.3	13.3
Polyacrylic acid	10.0	10.1

Table 1 shows that the material composition of both multilayer electrodes is similar, which leads to a good comparability. This result shows that the same mass is transferred with the same parameters when printing on the current collector or on a previously printed layer, even if the top of the previous layer has a slightly lower distance to the donor plate. A different donor plate was used to print each layer. Since the values show a good agreement, this means that a donor plate change does not affect the printing result. The electrodes have a silicon content of more than 12 % which is quite a good value to increase the capacity of the electrode.

Electrochemical analysis

After the electrodes were assembled in coin-cells against lithium they were electrochemically primed and cycled at C/10 for 50 times followed by a short C-rate analysis. The results of the electrochemical analysis are displayed in Figure 3.

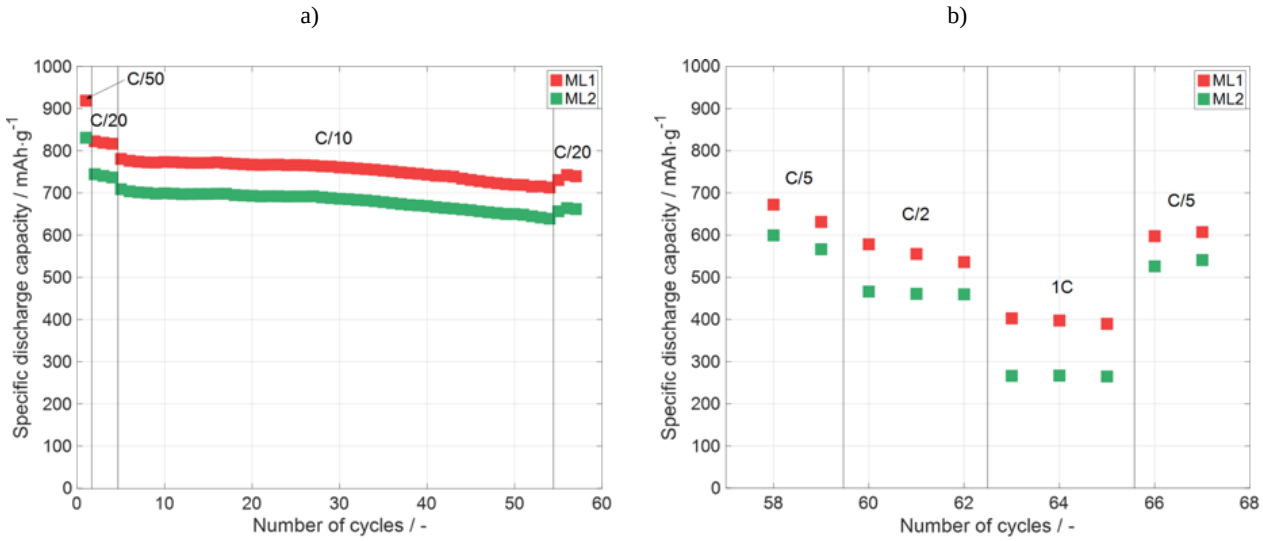

Figure 3: Specific discharge capacity of a) the long-term analysis at C/10 and b) the short C-rate analysis.

The specific discharge capacity of the electrochemical priming and long-term analysis at C/10 is displayed in Figure 3a over the number of cycles. Here, the specific capacity of the CCCV-phase is displayed. The cells with the ML1 electrode architecture (red) have a specific capacity of up to 817 $mAh \cdot g^{-1}$ at the end of the priming process, compared to up to 737 $mAh \cdot g^{-1}$ for the cells with the ML2 electrode architecture (green). Since the used graphite has a practical specific capacity of around 350 $mAh \cdot g^{-1}$ [15] the specific capacity of the manufactured electrodes was doubled by introducing silicon to the electrode. During the C/10 cycles the cells with the ML1 electrode architectures have a lower capacity fading than the cells with the ML2 electrode architectures. Subsequently to the C/10 cycles three C/20 cycles were performed to calculate the capacity retention after the 50 C/10 cycles. For this purpose, the specific capacity of the C/20 cycles are divided by the one of the C/20 cycles during the electrochemical priming. The capacity retention of ML1 is between 90.0 % and 92.6 % whereas the capacity retention of the ML2 cells is between 83.2 % and 90.8 %. It can be stated that when silicon is the bottom layer of a silicon-graphite multilayer the specific capacity and the cycle stability are higher. One explanation for this could be that the silicon closes the pores on the surface of the electrode, especially when the volume expansion took place due to the lithiation of silicon. With closed pores the diffusion of the lithium ions inside the electrode is hindered and the resistance of the battery is increasing. Subsequently to the long-term analysis a short C-rate analysis was performed, the results are displayed in Figure 3b. For the C-rate only the CC-phase of the lithiation process is depicted in the diagram. It can be seen, that at every C-rate the ML1 (red) have a higher specific discharge capacity than the ML2 cells (green). This can be explained by the same as the higher specific capacity in Figure 3a.

Post-mortem analysis

Subsequently to the C-rate analysis the cells were disassembled. Images of the electrodes front- and backside are displayed in Figure 4. Weather on the ML1 electrode shown in Figure 4a neither on the ML2 electrode displayed in Figure 4b a lithium plaiting can be observed on the surface of the electrode. In addition, the current collector on the backside of the electrodes do not show any deformation, which is in generally observed for unstructured silicon-containing electrodes as reported by Zheng et. al. [5]. This means that no failure mechanisms or material overstressing can be observed on the surface, even after 67 cycles and an amount of over 12 wt.% silicon within the electrode.

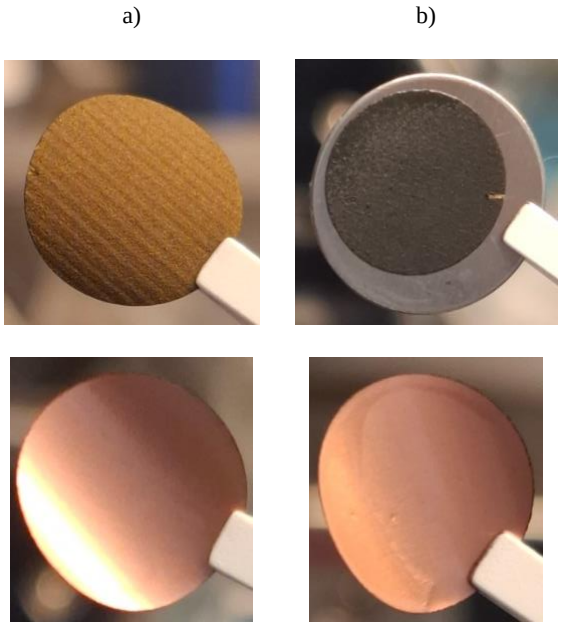

Figure 4: Images of the front- and backside of electrodes after the C-rate analysis, a) ML1 and b) ML2

4. CONCLUSION & OUTLOOK

Multilayer electrodes with different layer order were printed, containing one layer printed with graphite-containing ink and one layer printed with silicon-containing ink. A different donor plate was used for printing each layer, but since the material compositions of the printed electrodes match well, the change of the donor plates has no influence on the printing result. Subsequent to the printing, the electrodes were assembled into coin cells against lithium. Here, a specific capacity of up to 817 $mAh \cdot g^{-}1$ was reached. Thus, by introducing silicon into the electrode, the specific capacity of the electrodes could be doubled compared to a graphite-only electrode. After the priming process the cell with the electrode with the silicon-containing layer as bottom layer (ML1) had a higher specific capacity compared to the cell with the graphite layer as bottom layer (ML2). At the end of the C/10 long-term analysis the ML1 cells had a higher capacity retention compared to the ML2 cells which indicates a better cyclability. One explanation is that when silicon is at the top of the electrode the silicon closes the pores which hinder the lithium-ion diffusion. When the volume of the silicon particles increases due to the lithiation of silicon the effect would be amplified. After the electrochemical analysis the cells were disassembled. No lithium plating or a deformation of the current collector could be observed, which shows a good cyclability at the applied C-rates. Further studies should investigate the possibility of increasing the electrochemical performance with more than two layers and a larger variety of materials. Since LIFT is a digital additive manufacturing process, more complex geometries can be prepared and electrochemically characterized, for further electrode architecture research.

ACKNOWLEDGEMENT

We are grateful to our colleague Alexandra Reif for her support in SEM and LIBS measurements and to our colleague Marek Kapitz for ultrashort laser materials processing. This project has received funding from the German Research Foundation (DFG, 3D-Bat-Hybrid, project No. 467624762).

REFERENCES

[1] A. Baasner, F. Reuter, M. Seidel *et al.*, “The Role of Balancing Nanostructured Silicon Anodes and NMC Cathodes in Lithium-Ion Full-Cells with High Volumetric Energy Density,” Journal of The Electrochemical Society, 167(2), 020516-020527 (2020).

[2] W. Pfleging, “Recent progress in laser texturing of battery materials: a review of tuning electrochemical performances, related material development, and prospects for large-scale manufacturing,” International Journal of Extreme Manufacturing, 3(1), 012002-012022 (2021).
[3] W. Pfleging, “A review of laser electrode processing for development and manufacturing of lithium-ion batteries,” Nanophotonics, 7(3), 549-573 (2018).
[4] W. Pfleging, P. Gotcu, P. Smyrek *et al.*, “Lithium-Ion Battery—3D Micro-/Nano-Structuring, Modification and Characterization,” 309, 313-347 (2020).
[5] Y. Zheng, H. J. Seifert, H. Shi *et al.*, “3D silicon/graphite composite electrodes for high-energy lithium-ion batteries,” Electrochimica Acta, 317, 502-508 (2019).
[6] U. Rist, A. Reif, and W. Pfleging, "Laser-induced forward transfer as a versatile tool for developing silicon-based anode materials." 11989, 119890C1-119890C10.
[7] Z. Song, P. Zhu, W. Pfleging *et al.*, “Electrochemical Performance of Thick-Film Li(Ni0.6Mn0.2Co0.2)O2 Cathode with Hierarchic Structures and Laser Ablation,” Nanomaterials (Basel, Switzerland), 11, 2962-2977 (2021).
[8] L. Gottschalk, C. Oertel, N. Strzelczyk *et al.*, “Improving the Performance of Lithium-Ion Batteries Using a Two-Layer, Hard Carbon-Containing Silicon Anode for Use in High-Energy Electrodes,” Energy Technology, 11(5), 2200858-2200868 (2022).
[9] U. Rist, and W. Pfleging, [Laser-Induced Forward Transfer – Current Approaches and Perspectives for 4D Printing of Batteries], (2024).
[10] J. Holmström, M. Holweg, S. H. Khajavi *et al.*, “The direct digital manufacturing (r)evolution: definition of a research agenda,” Operations Management Research, 9(1-2), 1-10 (2016).
[11] P. Serra, and A. Piqué, [Introduction to Laser-Induced Transfer and Other Associated Processes] John Wiley & Sons Incorporated, Newark(2018).
[12] S. A. Mathews, R. C. Y. Auyeung, H. Kim *et al.*, “High-speed video study of laser-induced forward transfer of silver nano-suspensions,” Journal of Applied Physics, 114(6), 064910 (2013).
[13] H. Kim, R. C. Y. Auyeung, and A. Piqué, “Laser-printed thick-film electrodes for solid-state rechargeable Li-ion microbatteries,” Journal of Power Sources, 165(1), 413-419 (2007).
[14] P. Smyrek, H. Kim, Y. Zheng *et al.*, "Laser printing and femtosecond laser structuring of electrode materials for the manufacturing of 3D lithium-ion micro-batteries," SPIE Proceedings. 9738, 9738061-9738065.
[15] U. Rist, V. Falkowski, and W. Pfleging, “Electrochemical Properties of Laser-Printed Multilayer Anodes for Lithium-Ion Batteries,” Nanomaterials (Basel), 13(17), 1-20 (2023).
[16] U. Rist, F. Ball, and W. Pfleging, "3D printing of anode architectures for customized lithium-ion batteries." 12409, 124090N1-124090N7.
[17] H. Huang, “The Effect of Commercialized Binders on Silicon Oxide Anode Material for High Capacity Lithium ion Batteries,” International Journal of Electrochemical Science, 11, 8697-8708 (2016).
[18] B. Koo, H. Kim, Y. Cho *et al.*, “A Highly Cross-Linked Polymeric Binder for High-Performance Silicon Negative Electrodes in Lithium Ion Batteries,” Angewandte Chemie, 124(35), 8892-8897 (2012).
[19] A. Magasinski, B. Zdyrko, I. Kovalenko *et al.*, “Toward efficient binders for Li-ion battery Si-based anodes: polyacrylic acid,” ACS applied materials & interfaces, 2(11), 3004-3010 (2010).
[20] N. P. W. Pieczonka, V. Borgel, B. Ziv *et al.*, “Lithium Polyacrylate (LiPAA) as an Advanced Binder and a Passivating Agent for High-Voltage Li-Ion Batteries,” Advanced Energy Materials, 5(23), 1501008-1501017 (2015).
[21] C. C. Nguyen, T. Yoon, D. M. Seo *et al.*, “Systematic Investigation of Binders for Silicon Anodes: Interactions of Binder with Silicon Particles and Electrolytes and Effects of Binders on Solid Electrolyte Interphase Formation,” ACS applied materials & interfaces, 8(19), 12211-12220 (2016).
[22] J. M. Fernández-Pradas, C. Florian, F. Caballero-Lucas *et al.*, “Laser-induced forward transfer: Propelling liquids with light,” Applied Surface Science, 418, 559-564 (2017).
[23] U. Rist, Y. Sterzl, and W. Pfleging, "Laser-induced forward transfer (LIFT) process for flexible construction of advanced 3D silicon anode designs in high-energy lithium-ion batteries." 12873, 128730F1-128730F8.